Binding-Induced Formation of DNA Three-Way Junctions and Its Application to Protein Detection and DNA Strand Displacement

ARTICLE *in* ANALYTICAL CHEMISTRY · OCTOBER 2013

Impact Factor: 5.64 · DOI: 10.1021/ac402179a · Source: PubMed

3 AUTHORS, INCLUDING:

Feng Li
Brock University
25 PUBLICATIONS **1,145** CITATIONS
SEE PROFILE

X. Chris Le
University of Alberta
248 PUBLICATIONS **7,753** CITATIONS
SEE PROFILE

analytical chemistry

Article

pubs.acs.org/ac

Binding-Induced Formation of DNA Three-Way Junctions and Its Application to Protein Detection and DNA Strand Displacement

Feng Li,[†,‡] Yanwen Lin,[‡] and X. Chris Le*[,†,‡]

[†]Department of Laboratory Medicine and Pathology, University of Alberta, Edmonton, Alberta, Canada T6G 2G3

[‡]Department of Chemistry, University of Alberta, Edmonton, Alberta, Canada T6G 2G2

Supporting Information

ABSTRACT: DNA three-way junctions (DNA TWJs) are important building blocks to construct DNA architectures and dynamic assemblies. We describe here a binding-induced DNA TWJ strategy that is able to convert protein bindings to the formation of DNA TWJ. The binding-induced DNA TWJ makes use of two DNA motifs each conjugated to an affinity ligand. The binding of two affinity ligands to the target molecule triggers assembly of the DNA motifs and initiates the subsequent DNA strand displacement, resulting in a binding-induced TWJ. Real-time fluorescence monitoring of the binding-induced TWJ enables detection of the specific protein targets. A detection limit of 2.8 ng/mL was achieved for prostate-specific antigen. The binding-induced TWJ approach compares favorably with the toehold-mediated DNA strand-displacement, the associative (combinative) toehold-mediated DNA strand-displacement, and the binding-induced DNA strand-displacement. Importantly, the binding-induced TWJ broadens the scope of dynamic DNA assemblies and provides a new strategy to design protein-responsive DNA devices and assemblies.

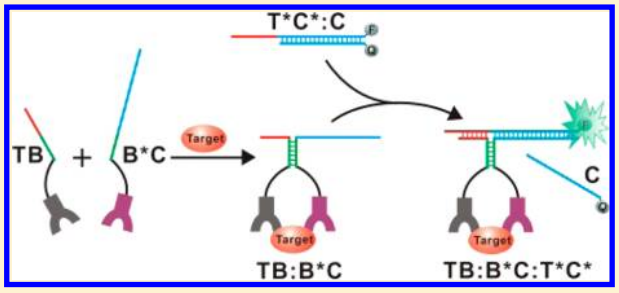

DNA three-way junctions (DNA-TWJs) are important building blocks to construct DNA architectures and dynamic assemblies.[1−9] Target-responsive DNA TWJs can also be designed into DNA devices for molecular diagnostic, sensing, and imaging applications.[10−14] Successful TWJs have been focused on DNA, but the benefits have not been extended to proteins because proteins do not possess the base-paring properties of DNA. We hypothesize that the affinity bindings between target molecules and their ligands can serve as a trigger to the formation of DNA TWJs. This binding-induced TWJ would provide a new strategy to design protein-responsive DNA devices and assemblies.

The principle of our binding-induced TWJ technology is inspired by the previous observation that two separate DNA strands that are linked by a stable DNA duplex can facilitate toehold-mediated DNA strand displacements (associative DNA toehold).[15−17] Although this TWJ strategy is highly successful for DNA, its application to proteins is challenging. Our innovation to confront this challenge leads to the development of a binding-induced TWJ technique (Scheme 1). Two DNA motifs, **TB** and **B*C**, are each conjugated with an affinity ligand. Motif **TB** is designed to have a toehold domain **T** and a binding domain **B**, separated by a flexible linker of two thymidine bases. Motif **B*C** has a binding domain **B*** and a competing domain **C**. **TB** and **B*C** are designed to have only 6 complementary bases (domain **B** and **B***, green color in Scheme 1), so that they cannot form a stable duplex at room temperature. However, in the presence of the target molecule, the binding of two affinity ligands to the same target molecule brings **TB** and **B*C** to close proximity, greatly increasing their local effective concentrations.[18] Consequently, **TB** and **B*C** hybridize to each other to form a stable **TB:B*C** duplex. Once **TB:B*C** forms, it triggers a subsequent toehold-mediated strand displacement reaction with **T*C*:C**, forming a binding-induced TWJ (**TB:B*C:T*C***) and releasing the motif **C**.

Scheme 1. Schematic Showing the Principle of the Binding-Induced Formation of DNA Three-Way Junction (TWJ)[a]

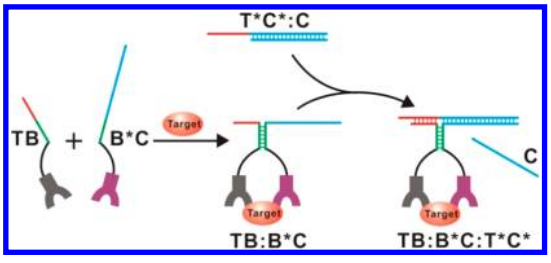

[a]Binding of the target molecule to the two specific affinity ligands brings two DNA motifs, **TB** and **B*C**, to close proximity, forming the **TB:B*C** duplex. The formation of **TB:B*C** triggers a subsequent strand displacement between **TB:B*C** and **C**, resulting in a stable binding-induced TWJ (**TB:B*C:T*C***) and the release of **C**. Symbols in this scheme do not reflect the actual sizes of the molecules.

Received: July 16, 2013
Accepted: October 19, 2013
Published: October 20, 2013

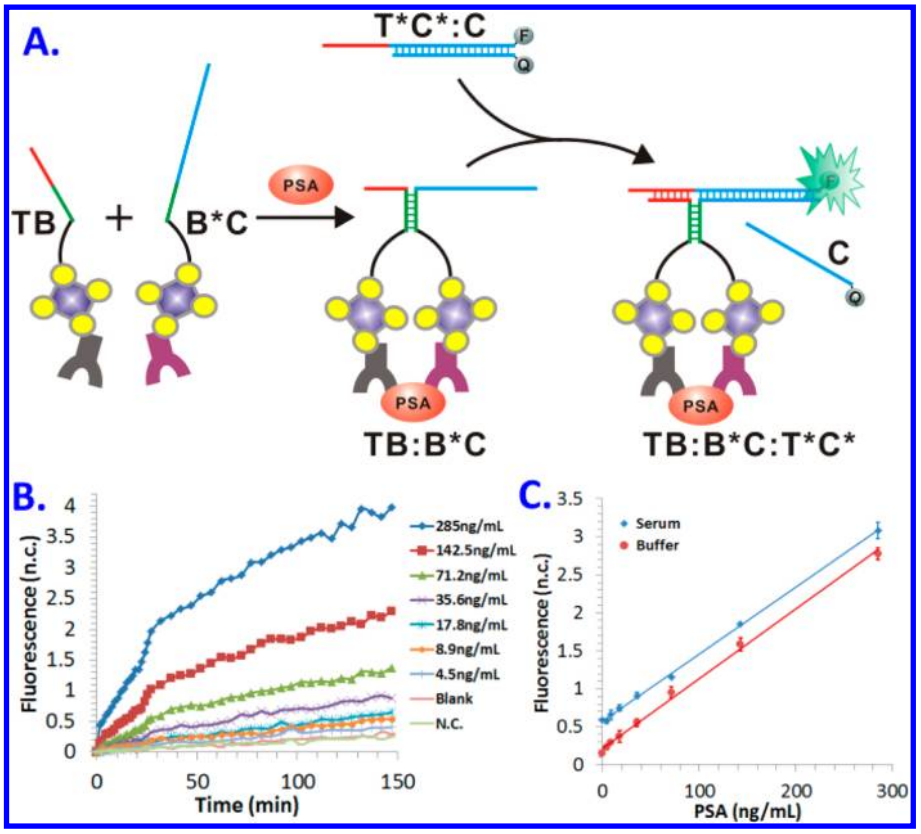

Figure 1. Detection of prostate-specific antigen (PSA) using binding-induced TWJ. (A) Schematic showing the design of PSA-responsive TWJ. (B) Real-time monitoring of the fluorescence increases over time from the determination of varying concentrations (0−285 ng/mL) of PSA. (C) Increases in fluorescence signals as a function of concentrations of PSA in buffer (red line) and in 10× diluted human serum (blue line). Fluorescence measurements were taken at 60 min.

EXPERIMENTAL SECTION

Materials and Reagents. Streptavidin from *Streptomyces avidinii* (product number, S4762), biotin (product number, B4501), bovine serum albumin (BSA), prostate-specific antigen from human semen (PSA), sterile-filtered human serum, magnesium chloride hexahydrate (MgCl2·6H2O), and 100× Tris−EDTA (TE, pH 7.4) buffer were purchased from Sigma (Oakville, ON, Canada). SYBR Gold and ROX Reference Dye (ROX) were purchased from Life Technologies (Carlsbad, CA). Biotinylated Human Kallikrein 3/PSA polyclonal antibody (goat IgG) was purchased from R&D Systems (Minneapolis, MN). Reagents for polyacrylamide gel electrophoresis (PAGE), including 40% acrylamide mix solution and ammonium persulfate, were purchased from BioRad Laboratories (Mississauga, ON, Canada). Tween 20 and 1,2-bis (dimethylamino)-ethane (TEMED) were purchased from Fisher Scientific (Nepean, ON, Canada). NANOpure H_2O (>18.0 M), purified using an Ultrapure Milli-Q water system, was used for all experiments. All DNA samples were purchased from Integrated DNA Technologies (Coralville, IA) and purified by high-performance liquid chromatography (HPLC). The DNA sequences and modifications are listed in Tables S1 and S2 of the Supporting Information.

Probe Preparation for Binding-Induced DNA Three-Way Junction. DNA probe (**T*C*:C**) for binding-induced TWJ (Table S1 of the Supporting Information) was prepared at a final concentration of 5 μM by mixing 20 μL of 50 μM FAM-labeled **T*C*** with 20 μL of 100 μM dark quencher-labeled **C** in 160 μL of TE−Mg buffer (1 × TE, 10 mM $MgCl_2$, 0.05% Tween20). The mixture was heated to 90 °C for 5 min and then the solution was allowed to cool down slowly to 25 °C in a period of 3 h. Probe (**T*C*:C**) for gel electrophoresis (Table S2 of the Supporting Information) was also prepared at a final concentration of 5 μM by mixing 20 μL of 50 μM unlabeled **T*C*** with 20 μL of 25 μM FAM-labeled **C** in 160 μL of TE−Mg buffer. Similarly, the solution was heated to 90 °C for 5 min and then cooled down to 25 °C slowly in a period of 3 h.

Real-Time Monitoring of the Toehold-Mediated DNA Strand Displacement. For a typical toehold-mediated DNA strand displacement reaction (Figure S1A of the Supporting Information), the reaction mixture contained 20 nM probe **T*C*:C**, 50 nM ROX reference dye, 1 μM polyT oligo, varying concentrations of the target DNA **TC** ($\mathbf{T_8C_{20}}$), and TE−Mg buffer. The reaction mixture was incubated at 25 °C for 45 min in a 96-well plate. Fluorescence was measured directly from the microplate using a multimode microplate reader (DX880, Beckman Coulter). The excitation/emission for the DNA probes were 485/515 nm and the excitation/emission for the ROX reference dye were 535/595 nm.

To monitor the kinetic process of toehold-mediated DNA strand displacement reaction (Figure S1B of the Supporting Information), we measured the fluorescence of the reaction mixture every 1.5 min for the first 30 min and then every 5 min for another 15 min. Figure S1B of the Supporting Information shows increases in the fluorescence signals over a period of 45 min from the toehold-mediated DNA strand displacement between 20 nM**T*C*:C** and **TC** (0−20 nM). A calibration between the fluorescence intensity and the concentration of **TC** is linear with the range of concentrations tested (1.25−20 nM, Figure S1C of the Supporting Information).

Binding-Induced TWJ Probes for Prostate Specific Antigen (PSA) and Human α-Thrombin. To prepare DNA probes for the detection of PSA using binding-induced TWJ, we mixed 25 μL of 2.5 μM biotinylated probe $\mathbf{T_9B_6}$ or probe **B*C** with equal volume of 2.5 μM streptavidin (diluted in 20 mM Tris buffer, containing 0.01% BSA) and then incubated the solution at 37 °C for 30 min, followed by incubation at 25 °C for another 30 min. To this reaction mixture, 50 μL of 1.25 μM biotinylated PSA polyclonal antibodies (diluted in 20 mM Tris buffer saline, containing 0.01% BSA) was then added. The solution was incubated at 25 °C for 30 min. The prepared DNA probe

dx.doi.org/10.1021/ac402179a | *Anal. Chem.* 2013, 85, 10835−10841

was then diluted to 250 nM with a solution containing 20 mM Tris buffer saline, 0.01% BSA, and 1 mM biotin.

Two distinct thrombin aptamer sequences (underlined in Table S2 of the Supporting Information) were added to the end of the **B*C** and T_9B_6 sequences, respectively (Table S1 of the Supporting Information), forming DNA probes (**B*C** and **TB** in Table S2 of the Supporting Information). These DNA sequences were obtained from Integrated DNA Technologies (Coralville, IA). They were used as the probes, as shown in Figure 2, for the detection of thrombin.

Detection of PSA and Thrombin Using Binding-Induced TWJ. For the detection of PSA and thrombin in buffer or in diluted human serum (Figure 1 and Figure 2), the reaction mixture contained

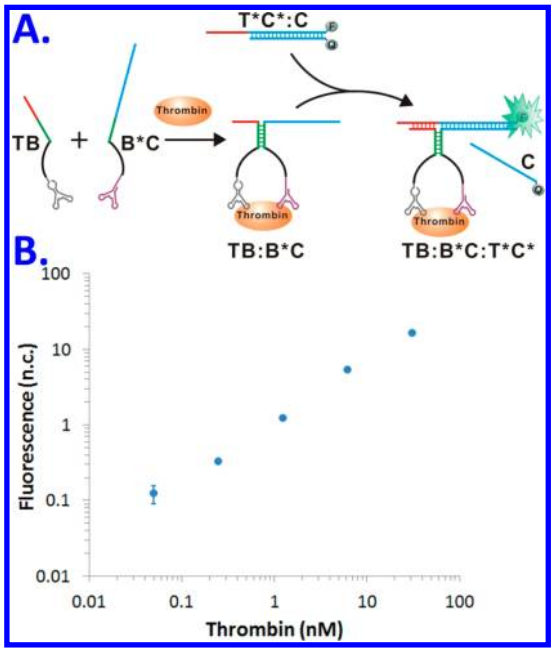

Figure 2. Detection of human α-thrombin using binding-induced TWJ. (A) Schematic showing the design of thrombin-responsive TWJ. (B) Increases in fluorescence signals as a function of concentrations of thrombin in a buffer solution. Fluorescence measurements were taken at 60 min.

20 nM antibody-modified or aptamer-modified probe **TB**, 20 nM antibody-modified or aptamer-modified probe **B*C**, 50 nM ROX reference dye, 1 μM polyT oligo, varying concentrations of the target proteins (PSA or thrombin), and TE−Mg buffer. The reaction mixture was incubated at 37 °C for 30 min and then transferred into a 96-well plate. Detection probe **T*C*:C** was then added to the reaction mixture at a final concentration of 20 nM. Fluorescence was measured every 1.5 min for the first 30 min and then every 5 min for another 2 h. Fluorescence was measured directly from the microplate using a multimode microplate reader (DX880, Beckman Coulter). The excitation/emission for DNA strand displacement were 485/515 and excitation/emission for ROX reference dye were 535/595 nm. The measured fluorescent signal was normalized so that 1 normalized unit (n.u.) of fluorescence corresponded to the fluorescent signal generated by 1 nM **TC**. This normalization was achieved using a positive control containing 10 nM **TC**, 20 nM **T*C*:C**, 1 μM polyT oligo, and 50 nM Rox in TE−Mg buffer and a negative control containing identical reagents in positive control except that there was no **TC** added.

The end-point detection of the target proteins (PSA and thrombin) was achieved by incubating the reaction mixture at 25 °C for 60 min in a PCR tube in the dark. The reaction mixture was then transferred to a 96-well microplate and fluorescence was measured using the multimode microplate reader as described above.

Monitoring the Formation of Binding-induced TWJ Using Gel Electrophoresis. A reaction mixture contained 2 μM probe **B*C**, 2 μM probe **TB**, 1 μM **T*C*:C**, 1 μM **T*C***, 1 μM target protein, and TE−Mg buffer. The reaction mixture was incubated at 25 °C for 30 min. After incubation, the reaction mixture was then assessed using 12% native polyacrylamide gel electrophoresis (PAGE). All the gels were freshly prepared in house. Before loading, DNA samples were mixed with DNA loading buffer on a volume ratio of 5:1. A potential of 12 V/cm was applied for gel electrophoresis separation.

After separation, PAGE gels were imaged using an ImageQuant 350 digital imaging system. Two approaches were used to measure the fluorescently labeled DNA and total DNA, separately. The PAGE gels were first imaged without any staining procedure, and therefore only the fluorescently labeled (FAM-labeled) DNA bands were visualized (Figure 3C). The same PAGE gels were then stained with SYBR Gold,

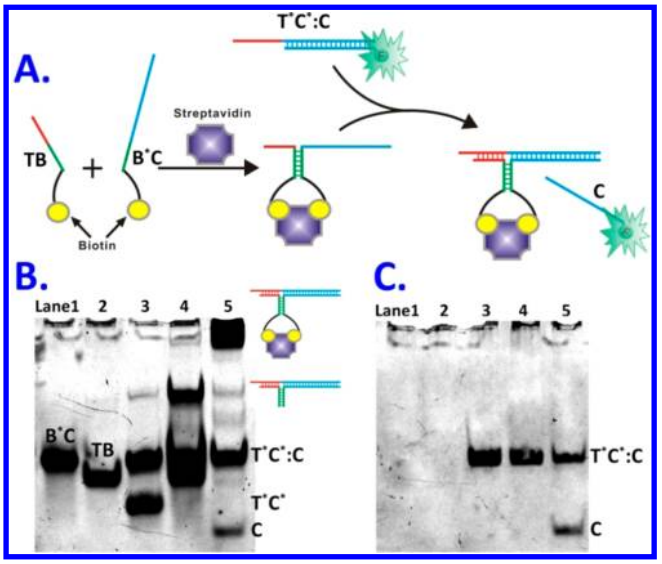

Figure 3. Characterization of the oligonucleotides involved in the formation of binding-induced TWJ and strand displacement. (A) Schematic showing that binding of the two probes to streptavidin triggers the formation of TWJ and the release of fluorescent oligo**C**. (B) Images of native PAGE gels after SYBR Gold staining. (C) Fluorescence images of native PAGE gels without staining. In this case, the bands correspond to FAM-labeled DNA. All native gel electrophoresis separation was performed at a potential of 12 V/cm. Lane 1 contained 2 μM **B*C**. Lane 2 contained 2 μM **TB**. Lane 3 contained 1 μM **T*C*:C** and 1 μM **T*C***. Lane 4 was from the analysis of a mixture containing 2 μM **B*C**, 2 μM TB, 1 μM**T*C*:C**, and 1 μM **T*C***. Lane 5 was from the analysis of a mixture containing 2 μM **B*C**, 2 μM **TB**, 1 μM **T*C*:C**, 1 μM**T*C***, and 1 μM streptavidin. The addition of **T*C*** was to hybridize it to any free **C**, thereby reducing potential background.

and images were taken again (Figure 3B). All DNA bands were detected using the second approach (i.e., after the SYBR Gold staining).

Real-Time Detection of Streptavidin Using Binding-Induced TWJ. For real-time detection of streptavidin using binding-induced TWJ, the reaction mixture contained 20 nM FAM-labeled probe **T*C*:C**, 20 nM probe **TB**, 20 nM probe **B*C**, 50 nM ROX reference dye, 1 μM polyT oligo, varying concentrations of the target streptavidin, and TE−Mg buffer. The reaction mixture was incubated at 25 °C in a 96-well microplate. Fluorescence was measured directly from the microplate every 1.5 min for the first 30 min and then every 5 min for another 2 h. The measured fluorescent signal was normalized so that 1 normalized unit (n.u.) of fluorescence corresponded to the fluorescent signal generated by 1 nM**TC**. This normalization was achieved using a positive control containing 10 nM**TC**, 20 nM**T*C*:C**, 1 μM polyT oligo, and 50 nM ROX reference dye in a TE−Mg buffer and a negative control containing identical reagents as in the positive control with the exception that there was no **TC** added. The rate constant k_{obs} was determined from the following equation:

dx.doi.org/10.1021/ac402179a | *Anal. Chem.* 2013, 85, 10835−10841

$\ln(1 - [\text{output}]/[\text{input}]) = k_{obs} \times t$, where [output] is the normalized fluorescence at each time point and [input] is the total normalized fluorescence corresponding to the concentrations of target added.

A calibration was generated from the analyses of solutions containing varying concentrations of streptavidin (Figure S2 of the Supporting Information). The reaction mixtures, as described above, were incubated in separate PCR tubes in the dark. The reaction mixture was then transferred into a 96-well microplate. Fluorescence was measured as described above.

Monitor the Kinetics of DNA Strand Displacement Mediated by Associative DNA Toehold. For monitoring the kinetics of DNA strand displacement mediated by associative DNA toehold, the reaction mixture contained 20 nM FAM-labeled probe **T*C*:C**, 10 nM probe $\mathbf{T_9B_{15}}$, 10 nM probe **B*C**, 50 nM ROX reference dye, 1 μM polyT oligo, and TE−Mg buffer. The reaction mixture was incubated at 25 °C in a 96-well plate. The subsequent fluorescence detection and signal normalization were the same as described above.

Monitor the Kinetics of Binding-Induced DNA Strand Displacement. For monitoring the kinetics of binding-induced DNA strand displacement, the reaction mixture contained 20 nM probe **Biotin-C*:C**, 20 nM probe **C-Biotin**, 10 nM target streptavidin, 50 nM ROX reference dye, 1 μM polyT oligo, and TE−Mg buffer. The reaction mixture was incubated at 25 °C in a 96-well plate. Fluorescence was measured every 1.5 min for the first 30 min and then every 5 min for another 2 h. The measured fluorescent signal was normalized so that 1 n.u. of fluorescence corresponded to the fluorescent signal generated by 1 nM**TC**. This normalization was achieved using a positive control containing 10 nM $\mathbf{T_8C_{15}}$, 20 nM **T*C*:C**, 1 μM polyT oligo, and 50 nM ROX in the TE−Mg buffer and a negative control containing identical reagents as in the positive control, with the exception that there was no $\mathbf{T_8C_{15}}$ added. The observed rate constant k_{obs} was determined as described above using the equation: $\ln(1 - [\text{output}]/[\text{input}]) = k_{obs} \times t$.

RESULTS AND DISCUSSION

Assay for Prostate Specific antigen (PSA). We first constructed a binding-induced TWJ as a sensor for prostate specific antigen (PSA) in human serum. We conjugated polyclonal anti-PSA antibodies to DNA motifs **TB** and **B*C** through streptavidin−biotin interactions (Figure 1A). We also modified DNA motifs by labeling **T*C*** with a fluorescent dye FAM and labeling **C** with a quencher. Because the FAM-labeled **T*C*** was initially hybridized with the quencher-labeled **C**, the fluorescence was quenched. However, in the presence of the target PSA, the binding of PSA to two antibodies brings **TB** and **B*C** together, resulting in the formation of the FAM-labeled binding-induced TWJ (**TB:B*C:T*C***) and the simultaneous release of the quencher-labeled **C** (Figure 1A). Thus, the binding-induced TWJ becomes fluorescent. By monitoring this fluorescence increase, we are able to quantify the amount of the target PSA in real-time.

Figure 1B shows the increases in fluorescence signal from the determination of PSA (0−285 ng/mL) using the binding-induced TWJ. The measured fluorescence increases over a period of 150 min are proportional to the concentrations of PSA ranging from 4.5 to 285 ng/mL (Figure 1B). A calibration between the fluorescence intensity and the concentration of PSA is linear within the range of concentrations tested (Figure 1C, red line). An estimated detection limit is 2.8 ng/mL.

Having constructed a binding-induced TWJ sensor for PSA, we further explored its ability to detect the target proteins in complicated sample matrix (e.g., human serum samples). We spiked PSA to a 10× diluted human serum and then quantified the PSA concentrations using the binding-induced TWJ sensor. As shown in Figure 1C, we have achieved similar detection sensitivity for PSA in human serum samples (blue line) as in buffer solutions (red line), suggesting that our binding-induced TWJ sensor can be applied to real-world sample analysis with no need for any separation.

A slight background increase was observed when comparing the two calibration curves generated from PAS in buffer and PSA spiked in serum. This small increase is mainly due to the background fluorescence from the serum samples. The slopes from the two calibration curves are comparable, suggesting that there is minimum matrix effect. Such ability to quantify minute amounts of PSA (ng/mL level) present in human serum samples, without need for any separation, suggests that our sensor is very specific to the target protein. Two characteristics of the binding-induced TWJ technique contribute to the high specificity: (i) the use of two affinity ligands to bind with the same target molecule and (ii) the assembly and formation of DNA TWJ is triggered by simultaneous binding of both affinity ligands to the single target molecule.

On the basis of the same principle and design as for the detection of PSA, we have also used biotin−streptavidin binding to achieve the detection of streptavidin (Figure S2 of the Supporting Information), a second example of protein detection. A linear calibration was achieved between 50 pM and 10 nM.

Assay for Human α-Thrombin. To further explore the versatility of our approach, we constructed another binding-induced TWJ sensor for the detection of human α-thrombin (Figure 2). We chose two DNA aptamers that can specifically bind to two distinct binding-epitopes on the same thrombin molecule. We directly extended the sequences of the two aptamers (underlined in Table S2 of the Supporting Information), by including the sequences of DNA motifs **TB** and **B*C**, respectively (Table S2 of the Supporting Information). Same as for the detection of PSA, we used the DNA motif **T*C*:C** that was labeled with fluorescent FAM on the **T*C*** strand and a quencher on the complementary **C** strand. The fluorescence of the DNA motif **T*C*:C** was initially quenched. However, the binding of the target thrombin to the two aptamers brings **TB** and **B*C** to the same molecule, forming the FAM-labeled binding-induced TWJ (**TB:B*C:T*C***) and simultaneously releasing the quencher-labeled **C** (Figure 2A). Release of the quencher-labeled **C** leaves the binding-induced TWJ fluorescent. The fluorescence increase, measured in real-time, reflects the amount of the target thrombin in the sample. As shown in Figure 2B, a calibration between the fluorescence intensity (background subtracted) and the concentration of thrombin is linear within the range of concentrations tested (50 pM to 30 nM, r^2 = 0.9848).

Key Design Parameters Influencing the Kinetics. The key to our success in constructing the real-time sensor for PSA is to achieve a fast DNA strand displacement between **TB:B*C** and **T*C*:C** upon the target binding while minimizing target-independent strand displacement. To fully understand the kinetics of the DNA strand displacement involved in the formation of binding-induced TWJ, we used streptavidin as a target and biotin as the affinity ligand to optimize the key reaction parameters (Figures 3 and 4).

By monitoring the released quencher-labeled **C** from **T*C*:C**, we confirmed the strand displacement between **TC** and **T*C*:C** (Figure S1 of the Supporting Information). Using gel electrophoresis, we further characterized the oligonucleotides and their associated products that were involved in the formation of the binding-induced TWJ and the process of

dx.doi.org/10.1021/ac402179a | Anal. Chem. 2013, 85, 10835−10841

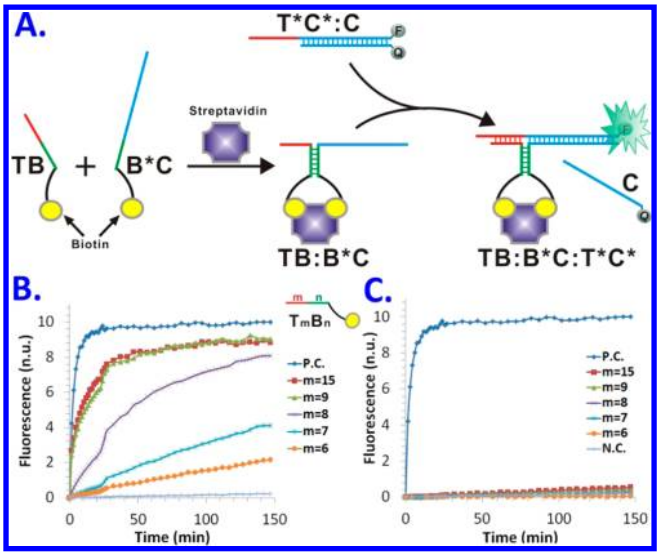

Figure 4. (A) Schematic showing the design for real-time monitoring of the formation of binding-induced TWJ. DNA motif **T*C*** was labeled with a fluorophore and motif **C** was labeled with a quencher. The fluorescently labeled **T*C*** was initially hybridized with **C**, thus its fluorescence was quenched by the quencher. Binding of the two biotinylated DNA motifs **TB** and **B*C** to the same target streptavidin triggered the formation of **TB:B*C:T*C*** TWJ and simultaneous release of the quencher-labeled **C**, turning on the fluorescence. (B and C) Optimizing the kinetics of binding-induced TWJ by using different designs of motif **TB** in the presence of 10 nM streptavidin (B) and in the absence of streptavidin (C). The length of the toehold domain **T** (m) was varied from 6 to 15 nt, and the length of domain **B** (n) was fixed at 6 nt. The positive control (P.C.) contained 10 nM probe $\mathbf{T_8C_{20}}$ and 20 nM **T*C*:C** in TE−Mg buffer. The negative control (N.C.) contained only 20 nM **T*C*:C** in TE−Mg buffer.

strand displacement. Figure 3 (panels B and C) show the characterization of relevant oligonucleotides using polyacrylamide gel electrophoresis (PAGE). The same gels were first directly imaged (Figure 3C), showing fluorescently labeled DNA, and then imaged again after staining with SYBR Gold (Figure 3B), showing all DNA. In the absence of the target streptavidin (lane 4), the incubation of **TB**, **B*C**, **T*C*:C**, and an excess amount of **T*C*** for 30 min leads to the formation of **TB:B*C:T*C*** (Figure 3B, lane 4). There is no observable band corresponding to **C** from either the direct fluorescence imaging (Figure 3C, line 4) or imaging after staining (Figure 3B, lane 4), confirming no release of **C**. However, in the presence of the target streptavidin (Figure 3B, lane 5), there is a strong band of the target-induced TWJ at the top of the lane and a clear band of **C**, indicating the formation of binding-induced TWJ and the strand displacement between **TB:B*C** and **T*C*:C**. In this set of experiments, all oligonucleotides were detected after the SYBR Gold staining (Figure 3B). We also directly imaged the native PAGE gels without using staining (Figure 3C). We labeled the motif **C** with the fluorescent dye FAM. Fluorescence detection of the gels revealed only the fluorescent **C** and its associated products, **T*C*:C**. Again, only in the presence of the target streptavidin, can the band of the released **C** be observed in the gel (Figure 3C, lane 5). These results confirm the strand displacement between **TB:B*C** and **T*C*:C** in response to the target binding. The use of an excess amount of **T*C*** in the experiments was to hybridize it to any free **C** in the absence of the target, thereby reducing the potential background.

We also monitored fluorescence in real time from the formation of the FAM-labeled TWJ product (Figure S2 of the Supporting Information). The fluorescence response is proportional to the concentration of the target proteins (0.16−10nM streptavidin).

In an effort to optimize the kinetics involved in the binding-induced TWJ processes, we designed the toehold domain **T** to have varied lengths from 6 nucleotides (nt) to 9 nt. As shown in Figure 4B, with the increase of the toehold length from 6 to 9 nt, the rate of fluorescence increase is accelerated 27×. This substantial enhancement is probably due to the increased kinetics for binding-induced strand displacement between **TB:B*C** and **T*C*:C**.[19] Increasing the length of toehold further from 9 to 15 nt does not lead to further increase in the reaction rate. Importantly, there is no noticeable background fluorescence signal increase for any of these designs, even after incubation for 150 min (Figure 4C), suggesting that our strategy is able to maintain an extremely low level of target-independent formation of TWJ.

To further maximize the speed of the binding-induced TWJ, we increased the reaction temperature from 25 to 37 °C. As shown in Figure 5, the increase in the reaction temperature

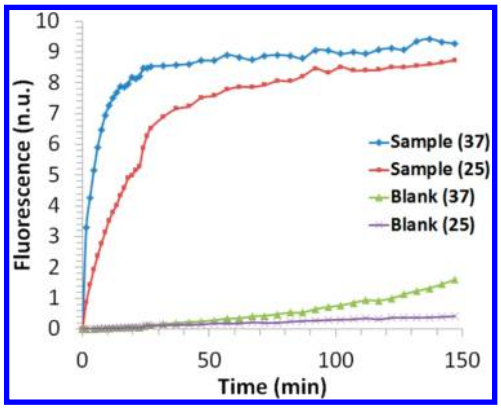

Figure 5. Effect of incubation temperature (37 and 25 °C) on the formation kinetics of binding-induced TWJ. The reaction mixture for the streptavidin sample contained 20 nM probe **T*C*:C**, 20 nM probe **TB**, 20 nM probe **B*C**, 10 nM target streptavidin, 50 nM ROX, 1 μM polyT oligo, and TE−Mg buffer. In the blank, all reagents were the same as in the sample solution, except that there was no streptavidin added.

accelerated the formation of binding-induced TWJ (k_{obs} = 1.58 × 10^{-3} s^{-1} at 37 °C and k_{obs} = 0.60 × 10^{-3} s^{-1} at 25 °C). Over 90% fluorescence signal was generated within 10 min. Although target-independent strand displacement between **B*C** and **T*C*:C** may be expected to increase with the increase in reaction temperature, our results show no noticeable background fluorescence increase until after 60 min, providing a time frame long enough for its potential applications (e.g., biomolecular sensing or imaging).

Comparison with DNA Strand-Displacement Strategies. Our success in constructing protein-responsive TWJs suggests that this strategy could potentially be adapted to existing dynamic DNA assemblies, including DNA logic gates,[20,21] molecular translators,[22−24] stepped DNA walkers,[25−27] and autonomous DNA machines.[28] To explore this potential, we compared (b) our technique with three other widely used DNA strand displacement strategies (Figure 6), (a) toehold-mediated DNA strand displacement,[19] (c) associative

dx.doi.org/10.1021/ac402179a | Anal. Chem. 2013, 85, 10835−10841

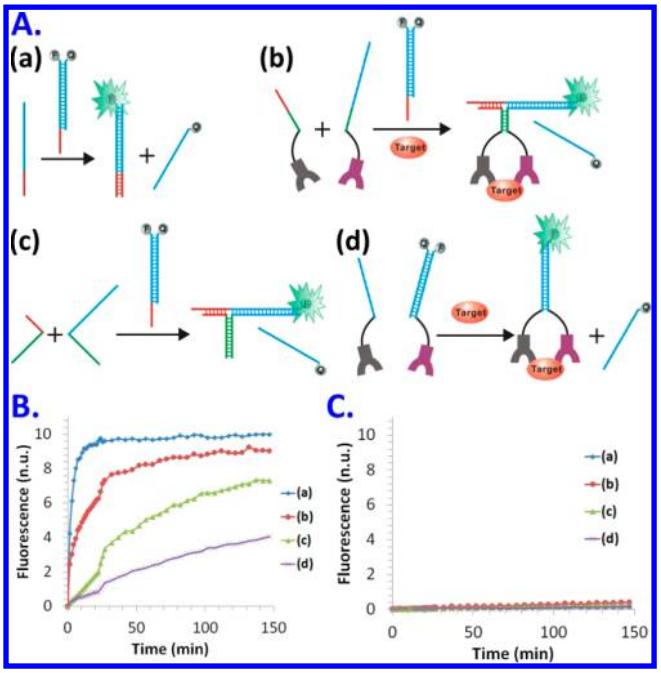

Figure 6. Comparison of four different DNA strand-displacement strategies and their kinetic profiles. (A) The four available strand-displacement strategies:[15−28] (a) toehold-mediated DNA strand displacement, (b) binding-induced TWJ, (c) DNA strand displacement mediated by associative DNA toehold, and (d) binding-induced DNA strand displacement. (B) Kinetic profiles from the determination of 10 nM target using the four strand-displacement strategies. (C) Background fluorescence observed from comparing the four strand−displacement strategies. The observed rate constant k_{obs} was (a) 3.31×10^{-3}, (b) 0.61×10^{-3}, (c) 0.16×10^{-3}, and (d) 0.06×10^{-3} s^{-1}.

DNA toehold (also known as combinatorial toehold)-mediated strand displacement,[15−17] and (d) binding-induced DNA strand displacement.[14] For a meaningful comparison, we used the identical duplex sequences (blue color) for all four techniques. In addition, (a−c) have the same DNA toehold sequences (red color); (b and d) have the same linker length (black color). Results in Figure 4B show the kinetic profiles of four DNA strand-displacement techniques in the presence of a 10 nM target DNA or protein. In comparison to other techniques, (b) our strategy exhibited fast reaction kinetics (ranked as the second fastest displacement reaction in Figure 6B) and an extremely low background from the target-independent displacement (Figure 6C). (a) The toehold-mediated DNA strand displacement[19−28] and (c) the associative (combinative) toehold-mediated DNA strand displacement[15−17] have been successfully used in dynamic DNA assemblies. With a kinetic profile positioned between those two successful techniques (Figure 6B), our (b) binding-induced TWJ technique can also have great potential to be applied in dynamic DNA assemblies. Importantly, the binding-induced TWJ broadens the scope of dynamic DNA assemblies to beyond DNA and to have the assemblies triggered by protein binding.

CONCLUSIONS

We have successfully developed a strategy to trigger the formation of DNA TWJs with specific proteins. The binding of two affinity ligands to the specific protein target triggers the assembly of DNA motifs and initiates the subsequent DNA strand displacement. Real-time fluorescence monitoring of the binding-induced TWJ provides sensitive detection of the specific proteins. The ability to generate detection signals with high sensitivity and fast kinetics in homogeneous solutions with no need for enzymes or thermal cycling makes this technique ideal for many emerging applications, such as point-of-care disease diagnostics and molecular imaging in live cells. The new approach to accelerate DNA strand-displacement reactions through affinity binding to specific proteins opens up opportunities to further expand the state-of-art DNA nanotechnology to proteins for diverse applications.

ASSOCIATED CONTENT

Supporting Information

Tables S1, S2, and S3 and Figures S1 and S2. This material is available free of charge via the Internet at http://pubs.acs.org.

AUTHOR INFORMATION

Corresponding Author

*E-mail: xc.le@ualberta.ca. Tel: 1-780-492-6416. Fax: 1-780-492-7800.

Notes

The authors declare no competing financial interest.

ACKNOWLEDGMENTS

This work was supported by the Natural Sciences and Engineering Research Council of Canada, the Canadian Institutes of Health Research, the Canada Research Chairs Program, Alberta Health, and Alberta Innovates.

REFERENCES

(1) Seeman, N. C. *J. Theor. Biol.* **1982**, *99*, 237−247.
(2) Seeman, N. C.; Kallenbach, N. R. *Annu. Rev. Biophys. Biomol. Struct.* **1994**, *23*, 53−86.
(3) Goodman, R. P.; Schaap, I. A. T.; Tardin, C. F.; et al. *Science* **2005**, *310*, 1661−1665.
(4) Yang, H.; Sleiman, H. F. *Angew. Chem., Int. Ed.* **2008**, *47*, 2443−2446.
(5) Boer, D. R.; Kerckhoffs, J. M. C. A.; Parajo, Y.; et al. *Angew. Chem., Int. Ed.* **2010**, *49*, 2336−2339.
(6) He, Y.; Chen, Y.; Liu, H.; Ribbe, A. E.; Mao, C. *J. Am. Chem. Soc.* **2005**, *127*, 12202−12203.
(7) Shu, D.; Shu, Y.; Haque, F.; Abdelmawla, S.; Guo, P. *Nat. Nanotechnol.* **2011**, *6*, 658−667.
(8) Muller, J.; Lippert, B. *Angew. Chem., Int. Ed.* **2006**, *45*, 2503−2505.
(9) Hamada, S.; Murata, S. *Angew. Chem., Int. Ed.* **2009**, *48*, 6820−6823.
(10) Thomas, J. M.; Chakraborty, B.; Sen, D.; Yu, H.-Z. *J. Am. Chem. Soc.* **2012**, *134*, 13823−13833.
(11) Seemann, I. T.; Singh, V.; Azarkh, M.; Drescher, M.; Hartig, J. S. *J. Am. Chem. Soc.* **2011**, *133*, 4706−4709.
(12) Thomas, J. M.; Yu, H.-Z.; Sen, D. *J. Am. Chem. Soc.* **2012**, *134*, 13738−13748.
(13) Ge, B.; Huang, Y. C.; Sen, D.; Yu, H.-Z. *Angew. Chem., Int. Ed.* **2010**, *49*, 9965−9967.
(14) Nutiu, R.; Li, Y. *J. Am. Chem. Soc.* **2003**, *125*, 4771−4778.
(15) Chen, X. *J. Am. Chem. Soc.* **2012**, *134*, 263−271.
(16) Li, B.; Jiang, Y.; Chen, X.; Ellington, A. D. *J. Am. Chem. Soc.* **2012**, *134*, 13918−13921.
(17) Genot, A. J.; Bath, J.; Turberfield, A. J. *Angew. Chem., Int. Ed.* **2013**, *52*, 1189−1192.
(18) Li, F.; Zhang, H.; Wang, Z.; Li, X.; Li, X.-F.; Le, X. C. *J. Am. Chem. Soc.* **2013**, *135*, 2443−2446.

(19) Zhang, D. Y.; Winfree, E. *J. Am. Chem. Soc.* **2009**, *131*, 17303−17314.
(20) Seelig, G.; Soloveichik, D.; Zhang, D. Y.; Winfree, E. *Science* **2006**, *314*, 1585−1588.
(21) Qian, L.; Winfree, E. *Science* **2011**, *332*, 1196−1201.
(22) Liao, S.; Seeman, N. C. *Science* **2004**, *306*, 2072−2074.
(23) Picuri, J. M.; Frezza, B. M.; Chadiri, M. R. *J. Am. Chem. Soc.* **2009**, *131*, 9368−9377.
(24) Li, F.; Zhang, H.; Lai, C.; Li, X.-F.; Le, X. C. *Angew. Chem., Int. Ed.* **2012**, *51*, 9317−9320.
(25) Shin, J.-S.; Pierce, N. A. *J. Am. Chem. Soc.* **2004**, *126*, 10834−10835.
(26) Gu, H.; Chao, J.; Xiao, S.-J.; Seeman, N. C. *Nature* **2010**, *465*, 202−205.
(27) He, Y.; Liu, D. R. *Nat. Nanotechnol.* **2010**, *5*, 778−782.
(28) Bath, J.; Turberfield, A. J. *Nat. Nanotechnol.* **2007**, *2*, 275−284.